Research Paper
Computational Methods for Differential Equations
http://cmde.tabrizu.ac.ir
Vol. *, No. *, *, pp. 1-25
DOI:10.22034/cmde.2026.70358.3490

Numerical simulation of Oncolytic M1 cancer Virotherapy reaction-diffusion model by finite element method

Hero M. Hussein[1] **and Younis A. Sabawi**[1,2,*]

[1]Department of Mathematics, Faculty of Science and Health, Koya University, Koya KOY45, Kurdistan Region - F.R. Iraq.

[2]College of Information Technology, Imam Ja'afar AL-Sadiq University, Baghdad, Iraq.

Abstract

This paper presents a finite element analysis of the reaction-diffusion system modeling oncolytic M1 virotherapy. The governing PDEs describe coupled biological interactions between tumor cells, viruses, and immune components through nonlinear reaction terms and diffusion processes. We develop a semi-discrete Galerkin formulation, establishing existence, uniqueness, and convergence of solutions. A comprehensive sensitivity analysis evaluates parameter influences through non-normalized, half-normalized, and fully normalized measures, identifying critical therapeutic parameters including viral replication rate (μ) and tumor-virus interaction coefficients (β_3). The numerical implementation demonstrates robust handling of system nonlinearities while preserving key conservation properties. Computational results validate the method's accuracy in capturing spatiotemporal dynamics, particularly in solving emergent patterns in tumor-virus interactions. The framework provides an effective computational tool for predicting therapeutic outcomes and optimizing treatment parameters in heterogeneous tumor environments, with sensitivity results guiding parameter prioritization for clinical translation.

Keywords. Finite element method, Reaction-diffusion system, Oncolytic virotherapy, Sensitivity analysis, Cancer modeling, Numerical simulation.
2010 Mathematics Subject Classification. 45L05, 74S05, 93A30.

1. Introduction

Cancer remains one of the most formidable challenges in modern medicine, accounting for millions of deaths worldwide annually. Among emerging therapeutic modalities, oncolytic virotherapy has emerged as a promising biological intervention strategy, leveraging genetically modified viruses to selectively target and lyse malignant cells while preserving healthy tissue architecture. The M1 strain of oncolytic alphavirus has demonstrated particular therapeutic potential due to its inherent tropism for transformed cells and capacity for intratumoral amplification. However, the spatiotemporal dynamics of viral spread, tumor regression, and host immune responses constitute a complex nonlinear system requiring rigorous mathematical formalization.

Reaction-diffusion partial differential equations (PDEs) provide a robust mathematical framework for modeling these biological interactions, capturing both local reaction kinetics and spatial transport phenomena. The model proposed by Elaiw et al. [4] extends previous formulations by incorporating cytotoxic T-lymphocyte (CTL) immune responses and diffusive transport, yielding a coupled system of five nonlinear PDEs governing nutrient dynamics ($\mathcal{H}$), normal cell populations ($\mathcal{N}$), tumor cell densities ($\mathcal{Y}$), viral particle distribution ($\mathcal{V}$), and immune effector cell concentrations ($\mathcal{Z}$). While prior numerical approaches have employed collocation methods, the finite element method (FEM) offers distinct advantages for this class of problems, particularly in handling heterogeneous material properties and complex boundary conditions inherent to biological systems.

To better understanding of the complex dynamics in oncolytic virotherapy, several mathematical models have been developed [8, 13]. These models share similarities with those describing HBV and HIV viral infections [14], and are designed to improve the analysis of cancer treatment approaches. Wang et al. [22] investigated how virus burst size

Received: 23 November 2025; Accepted: 28 July 2026.
∗ Corresponding author. Email: younis.abid@koyauniversity.org.

impacts viral therapy outcomes. Additionally, Malinzi et al. [8] developed a model to evaluate the effectiveness of combining oncolytic virotherapy with chemotherapy, demonstrating that this dual approach could be more beneficial when optimal dosage levels are administered.

Tumwiine *et al.* [21] analyzed an intra-host malaria model, examining interactions between parasites, red blood cells, and immune effectors. They proved global stability: the disease-free equilibrium is stable if $\mathcal{R}_0 \leq 1$, while an endemic equilibrium exists and is stable if $\mathcal{R}_0 > 1$. Numerical results showed immune response can destabilize the endemic state. Elaiw *et al.* [4] studied an oncolytic M1 virotherapy model with immune response and diffusion. They analyzed equilibria, stability, and thresholds for treatment success, showing that immune reactions may reduce therapeutic efficacy.

In [1], they solved the Allen–Cahn equation using a non-lumping Galerkin FEM with Crank–Nicolson time stepping. They derived error estimates, proved stability, and demonstrated high accuracy in numerical tests. From [15, 18], they solved the Whitham–Broer–Kaup shallow water model using a cubic B-spline FEM. They proved solution uniqueness, derived convergence estimates, and validated the method with numerical tests, showing high accuracy in L^2 and L^∞ norms. A posteriori error analysis for semilinear parabolic problems was developed using backward Euler FEM and elliptic reconstruction, handling both Lipschitz and non-Lipschitz nonlinearities, in[12, 17].

The present work develops a comprehensive FEM framework for the oncolytic virotherapy system, establishing rigorous theoretical foundations while demonstrating practical computational efficacy. Our approach makes three principal contributions to the field: We derive a semi-discrete Galerkin formulation and prove existence, uniqueness, and convergence properties in appropriate Sobolev spaces, addressing the challenges posed by the system's nonlinear coupling and degenerate diffusion. Computational results elucidate pattern formation mechanisms in tumor-virus-immune interactions, providing quantitative tools for treatment optimization in heterogeneous tumor microenvironments.

The paper is organized as follows: Section 2 presents the semi-discrete formulation and theoretical analysis, Section 3 details the finite element implementation, Section 4 examines parameter sensitivity through normalized measures, and Section 5 demonstrates computational results across various therapeutic scenarios. Our findings demonstrate that the FEM framework provides an effective computational tool for predicting therapeutic outcomes and optimizing treatment parameters, advancing the quantitative understanding of oncolytic virotherapy dynamics.

The reaction-diffusion model for oncolytic M1 virotherapy with immune response is given by:

$$\frac{\partial \mathcal{H}}{\partial t} = D_{\mathcal{H}}\Delta\mathcal{H} + \kappa - d\mathcal{H} - \beta_1\mathcal{H}\,\mathcal{N} - \beta_2\mathcal{H}\mathcal{Y} \tag{1.1a}$$

$$\frac{\partial \mathcal{N}}{\partial t} = D_{\mathcal{N}}\Delta\mathcal{N} + \alpha_1\beta_1\mathcal{H}\,\mathcal{N} - (d+\eta_1)\mathcal{N} \tag{1.1b}$$

$$\frac{\partial \mathcal{Y}}{\partial t} = D_{\mathcal{Y}}\Delta\mathcal{Y} + \alpha_2\beta_2\mathcal{H}\mathcal{Y} - \beta_3\mathcal{Y}\mathcal{V} - \beta_4\mathcal{Y}\mathcal{Z} - (d+\eta_2)\mathcal{Y} \tag{1.1c}$$

$$\frac{\partial \mathcal{V}}{\partial t} = D_{\mathcal{V}}\Delta\mathcal{V} + \mu + \alpha_3\beta_3\mathcal{Y}\mathcal{V} - (d+\eta_3)\mathcal{V} \tag{1.1d}$$

$$\frac{\partial \mathcal{Z}}{\partial t} = D_{\mathcal{Z}}\Delta\mathcal{Z} + \alpha_4\beta_4\mathcal{Y}\mathcal{Z} - (d+\eta_4)\mathcal{Z} \tag{1.1e}$$

for time $t > 0$ and position $x \in \Omega$, the system is governed by five state variables: $\mathcal{H}(x,t)$ (nutrient concentration), $\mathcal{N}(x,t)$ (normal cell density), $\mathcal{Y}(x,t)$ (tumor cell density), $\mathcal{V}(x,t)$ (free M1 virus concentration), and $\mathcal{Z}(x,t)$ (CTL cell density). The domain Ω is continuous and bounded with smooth boundary $\partial\Omega$. The model incorporates three key biological processes: CTL-mediated tumor cell lysis occurring at rate $\beta_4\mathcal{Y}\mathcal{Z}$, tumor-induced CTL proliferation with rate $\alpha_4\beta_4\mathcal{Y}\mathcal{Z}$, and natural CTL death at rate $\eta_4\mathcal{Z}$. The spatial dynamics are modeled through diffusion terms $D_U\Delta U$ for each component $U \in \{H, N, Y, V, Z\}$, where D_U represents the diffusion coefficient and Δ denotes the Laplacian operator. Initial conditions are specified by non-negative functions:

$$\mathcal{H}(x,0) = \phi_1(x), \qquad \mathcal{N}(x,0) = \phi_2(x),$$
$$\mathcal{Y}(x,0) = \phi_3(x), \qquad \mathcal{V}(x,0) = \phi_4(x),$$
$$\mathcal{Z}(x,0) = \phi_5(x), \qquad x \in \Omega$$

TABLE 1. Parameters and descriptions for the oncolytic M1 virotherapy model.

Parameter	Description
κ	Nutrient supply rate
μ	Viral production rate
d	Natural death rate
α_1	Conversion rate for normal cells
α_2	Conversion rate for tumor cells
α_3	Viral replication rate
α_4	CTL stimulation rate
β_1	Nutrient uptake rate by normal cells
β_2	Nutrient uptake rate by tumor cells
β_3	Viral infection rate of tumor cells
β_4	CTL attack rate on tumor cells
η_1	Death rate of normal cells
η_2	Death rate of tumor cells
η_3	Death rate of free viruses
η_4	Death rate of CTLs
$D_{\mathcal{H}}$	Nutrient diffusion coefficient
$D_{\mathcal{N}}$	Normal cells diffusion coefficient
$D_{\mathcal{Y}}$	Tumor cells diffusion coefficient
$D_{\mathcal{V}}$	Free viruses diffusion coefficient
$D_{\mathcal{Z}}$	CTLs diffusion coefficient

with homogeneous Neumann boundary conditions:

$$\frac{\partial \mathcal{H}}{\partial x} = \frac{\partial \mathcal{N}}{\partial x} = \frac{\partial \mathcal{Y}}{\partial x} = \frac{\partial \mathcal{V}}{\partial x} = \frac{\partial \mathcal{Z}}{\partial x} = 0, \quad t > 0, \quad x \in \partial\Omega$$

These no-flux conditions model biological containment, preventing cellular or viral transport across domain boundaries [23].

2. Semi-Discrete Galerkin Scheme

Consider an open set $\Omega \subset \mathbb{R}$ being bounded, and assume that all the functions presented in this study have real values. The space $C_c^\infty(\Omega)$ comprises infinitely differentiable functions that possess compact support inside Ω. The standard notation for Sobolev spaces is $W_p^r(\Omega)$; see [11] for further details. The Hilbert spaces are the Sobolev spaces $W_2^r(\Omega)$ for $p = 2$, which are denoted by $H^r(\Omega)$ to indicate their specific structure in this context. In $\mathbb{R}$, $D^\eta\phi$ represents the ηth derivative of ϕ. For H^r, the norm and semi-norm are represented by $\|\cdot\|_r$ and provided by:

$$\|\phi\|_r = \left(\sum_{|\eta| \le r} \int_\Omega (D^\eta \phi)^2 d\Omega \right)^{1/2}.$$

We are especially interested in the space $H^1(\Omega)$ for $r = 1$. The $H_0^1(\Omega)$ represents the completeness of $C_c^\infty(\Omega)$ in H^1 norm; in other words, $H_0^1(\Omega)$ includes those functions of $H^1(\Omega)$ that disappear at the boundary $\partial\Omega$. We shall write $\|\cdot\|$ for $\|\cdot\|_{L^2(\Omega)}$ for convenience. $(\cdot,\cdot)$ represents the inner product on L^2, whereas $\langle\cdot,\cdot\rangle$ represents the duality product on Hilbert spaces. $L^q(0,T;W_p^r(\Omega))$ is a representation of time dependent Sobolev spaces, which have the following formula:

$$L^q(0,T;W_p^r(\Omega)) = \left\{ \phi : (0,T) \to W_p^r(\Omega) \text{ s.t. } \phi \text{ is measurable and } \int_0^T \|\phi(t)\|_{W_p^r(\Omega)}^q dt < \infty \right\}$$

for any integer $r \geq 0$, $1 \leq q < \infty$, $1 \leq p \leq \infty$, using the subsequent norm,

$$\|\phi\|_{L^q(\Omega)} = \left(\int_0^T \|\phi(t)\|^q_{W^r_p(\Omega)} dt \right)^{1/q}, \text{ and } \|\phi\|_{H^1(\Omega)} = \left(\|\phi\|^2_{L^2(\Omega)} + \|\frac{\partial \phi}{\partial t}\|^2_{L^2(\Omega)} \right)^{1/2}.$$

This space consists of functions ϕ that exhibit both spatial and temporal regularity.

It is important to emphasize that the time-dependent norms $L^2(0,T;H^r(\Omega))$ should not be conflated with the standard spatial norm $L^2(\Omega)$. While $L^2(\Omega)$ measures integrability strictly over the spatial domain Ω, the norms $L^2(0,T;H^r(\Omega))$ represent integrability in both the temporal and spatial sense, accounting for the time evolution of the function over $(0,T)$ and the H^r-based spatial regularity on Ω.

Our use of some significant inequalities, like Young's inequality, Cauchy-Schwarz inequality, Poincaré's inequality, Gronwall's inequality, generalized Hölder's inequality, etc., is based on PDEs [5] and the standard text of functional analysis [6, 7].

We can write the system (1.1) in vector form as follows:

$$\frac{\partial U}{\partial t} = D_U * \Delta U + f(U), \tag{2.1}$$

where the symbol * denotes the componentwise multiplication of two vectors, with initial condition and homogeneous Neumann boundary condition are

$$U_i(x,0) = \phi_i(x), \quad \text{and } \nabla U_i = 0 \quad \text{on } \partial\Omega, \quad \text{for all } i = 1, \ldots, 5,$$

where

$$U = \begin{bmatrix} U_1 \\ U_2 \\ U_3 \\ U_4 \\ U_5 \end{bmatrix} = \begin{bmatrix} \mathcal{H} \\ \mathcal{N} \\ \mathcal{Y} \\ \mathcal{V} \\ \mathcal{Z} \end{bmatrix}, D_U = \begin{bmatrix} D_{U_1} \\ D_{U_2} \\ D_{U_3} \\ D_{U_4} \\ D_{U_5} \end{bmatrix} = \begin{bmatrix} D_{\mathcal{H}} \\ D_{\mathcal{N}} \\ D_{\mathcal{Y}} \\ D_{\mathcal{V}} \\ D_{\mathcal{Z}} \end{bmatrix},$$

$$f(U) = \begin{bmatrix} f_1(U) \\ f_2(U) \\ f_3(U) \\ f_4(U) \\ f_5(U) \end{bmatrix} = \begin{bmatrix} \kappa - \beta_1 \mathcal{H}\,\mathcal{N} - \beta_2 \mathcal{H}\mathcal{Y} - d\,U \\ \alpha_1\beta_1 \mathcal{H}\,\mathcal{N} - (d+\eta_1)U \\ \alpha_2\beta_2 \mathcal{H}\mathcal{Y} - \beta_3 \mathcal{Y}\mathcal{V} - \beta_4 \mathcal{Y}\mathcal{Z} - (d+\eta_2)U \\ \mu + \alpha_3\beta_3 \mathcal{Y}\mathcal{V} - (d+\eta_3)U \\ \alpha_4\beta_4 \mathcal{Y}\mathcal{Z} - (d+\eta_4)U \end{bmatrix},$$

Multiply (2.1) by a weight function $w \in H^1_0(\Omega)$, and integrated over Ω w.r.t. x and using integration by parts on the term involving ΔU, and $\nabla U = 0$ on $\partial\Omega$. Therefore, the weak formulation of the problem (2.1) can be written as:

$$(\frac{\partial U_i}{\partial t}, w) + D_{U_i}(\nabla U_i, \nabla w) = (f_i(U), w), \quad \text{for all } i \in \{1, \ldots, 5\}, \tag{2.2}$$

with the initial condition

$$(U_i(x,0), w) = (U_{i,0}(x), w).$$

where $(\gamma f, g) = \int_\Omega \gamma f(x,t) g(x,t)\, dx$. Let $S_h(\Omega), 0 < h < 1$, be a finite-dimensional subspace of $H^r_0(\Omega)$. A semi-discrete finite element Galerkin formulation of (2.2) is then defined as: find $U_{i,h} = U_{i,h}(x,t)$ belonging to S_h, such that

$$(\frac{\partial U_{i,h}}{\partial t}, w) + D_{U_i}(\nabla U_{i,h}, \nabla w) = (f_i(U_h), w), \quad \text{for all } i \in \{1, \ldots, 5\}, \tag{2.3}$$

with the initial condition

$$U_{i,h}(0) = U_{i,0h}, \forall w \in S_h, \tag{2.4}$$

where $U_{i,0h}$ is an approximation of $U_{i,0}$ in S_h.

2.1. **Existence and Uniqueness.** In this section, we will discuss the existence and uniqueness of the solution of the semi-discrete formulation (2.3).

Theorem 2.1. *For each component $i = 1, \dots, 5$, there exists a unique solution of the i^{th} equation of the semi-discrete formulation (2.3) with (2.4) for any $T > 0$ such that*

$$U_i \in L^\infty(0, T; H_0^1(\Omega)) \text{ with } (U_i(x, 0), w) = (U_{i,0}, w),\ w \in H_0^1(\Omega),$$

if $U_{i,0} \in H_0^1(\Omega)$ for any $T > 0$.

Proof. For each $m \in \mathbb{N}$, consider the finite-dimensional subspace $S_h^m \subset H_0^1(\Omega)$ spanned by eigenfunctions $\{\phi_j\}_{j=1}^m$ of the Laplacian. For each component $i = 1, \dots, 5$, we seek approximate solutions:

$$U_{i,h}^m(x, t) = \sum_{j=1}^{m} c_{i,j}^m(t)\phi_j(x),$$

satisfying for all $1 \le k \le m$:

$$\left(\frac{\partial U_{i,h}^m}{\partial t}, \phi_k\right) + a(U_{i,h}^m, \phi_k) = (f_i(U_h^m), \phi_k), \tag{2.5}$$

with initial conditions $U_{i,h}^m(0) = P^m U_{i,0}$, where P^m is the L^2-projection onto S_h^m. Hence (2.5) can be written as a system of first order non-linear ordinary differential equation and there exists a positive time $t_m > 0$ such that the nonlinear system has a unique solution U_i^m over $(0, t_m)$. Hence, $U_{i,h}^m$ can be defined by the standard existence and uniqueness theorem for system of ODEs [3]. Thus there exist $v_{i,h}^m \in S_h(\Omega)$ and $t_n \in (0, T]$.

To prove uniqueness, for each component $i = 1, \dots, 5$, let $U_{i,h}$ and $\tilde{U}_{i,h}$ be two solutions of i^{th} equation of (2.3) in S_h and take $V_i = U_{i,h} - \tilde{U}_{i,h}$, and subtracting the two resulting equations for the i^{th} equation, leads to

$$(\frac{\partial V_i}{\partial t}, w) + D_{U_i}(\nabla V_i, \nabla w) = (f_i(U_h) - f_i(\tilde{U}_h), w). \tag{2.6}$$

Choose $w = V_i$ in i^{th} equation of (2.6), we get

$$(\frac{\partial V_i}{\partial t}, V_i) + D_{U_i}(\nabla V_i, \nabla V_i) = (f_i(U_h) - f_i(\tilde{U}_h), V_i). \tag{2.7}$$

From (2.7), we have: $\frac{1}{2}\frac{d}{dt}\|V_i\|^2 + D_{U_i}\|\nabla V_i\|^2 = (f_i(U_h) - f_i(\tilde{U}_h), V_i)$.
Using the Cauchy-Schwarz inequality component-wise:

$$\frac{1}{2}\frac{d}{dt}\|V_i\|^2 + D_{U_i}\|\nabla V_i\|^2 \le \|f_i(U_h) - f_i(\tilde{U}_h)\|\|V_i\|$$

So, we have

$$\frac{1}{2}\frac{d}{dt}\|V_i\|^2 \le \|f_i(U_h) - f_i(\tilde{U}_h)\|\|V_i\|. \tag{2.8}$$

From the definition of f_i and the boundedness of $U_{i,h}$ and $\tilde{U}_{i,h}$, for all $i \in \{1, \dots, 5\}$, it follows that

$$\|f_1(U) - f_1(\tilde{U})\| = \left\|-\beta_1(\mathcal{HN} - \tilde{\mathcal{H}}\tilde{\mathcal{N}}) - \beta_2(\mathcal{HY} - \tilde{\mathcal{H}}\tilde{\mathcal{Y}}) - d(\mathcal{H} - \tilde{\mathcal{H}})\right\|.$$

Using the identity $\mathcal{HN} - \tilde{\mathcal{H}}\tilde{\mathcal{N}} = \mathcal{H}(\mathcal{N} - \tilde{\mathcal{N}}) + \tilde{\mathcal{N}}(\mathcal{H} - \tilde{\mathcal{H}})$, we bound the terms:

$$\|\mathcal{HN} - \tilde{\mathcal{H}}\tilde{\mathcal{N}}\| \le \|\mathcal{H}\|\|\mathcal{N} - \tilde{\mathcal{N}}\| + \|\tilde{\mathcal{N}}\|\|\mathcal{H} - \tilde{\mathcal{H}}\|.$$

Since, there exists $M > 0$ such that $\|U_{i,h}\|, \|\tilde{U}_{i,h}\| \le M$ for all i. Thus:

$$\|f_1(U_h) - f_1(\tilde{U}_h)\| \le \beta_1 M(\|\mathcal{N} - \tilde{\mathcal{N}}\| + \|\mathcal{H} - \tilde{\mathcal{H}}\|) + \beta_2 M(\|\mathcal{Y} - \tilde{\mathcal{Y}}\| + \|\mathcal{H} - \tilde{\mathcal{H}}\|) + d\|\mathcal{H} - \tilde{\mathcal{H}}\|.$$

Therefore, we have

$$\begin{aligned}\|f_1(U_h) - f_1(\tilde{U}_h)\| &\le (\beta_1 M + \beta_2 M + d)\|\mathcal{H} - \tilde{\mathcal{H}}\| + \beta_1 M\|\mathcal{N} - \tilde{\mathcal{N}}\| + \beta_2 M\|\mathcal{Y} - \tilde{\mathcal{Y}}\|. \\ &\le (\beta_1 M + \beta_2 M + d)\|V_1\| + \beta_1 M\|V_2\| + \beta_2 M\|V_3\|,\end{aligned}$$

$$\leq C\Big(\|V_1\| + \|V_2\| + \|V_3\|\Big),$$
$$\leq C\sum_{i=1}^{5}\|V_i\|$$

where C denotes a constant. Throughout this work, C will represent a generic constant and does not depend on h, which may take different values in different contexts.

Similarly, we do the similar steps for the other components, so from our component-wise Lipschitz estimates:

$$\|f_2(U_h) - f_2(\tilde{U}_h)\| \leq \alpha_1\beta_1 M\|V_1\| + (\alpha_1\beta_1 M + d + \eta_1)\|V_2\| \leq C\sum_{i=1}^{5}\|V_i\|.$$
$$\|f_3(U_h) - f_3(\tilde{U}_h)\| \leq \alpha_2\beta_2 M\|V_1\| + (\alpha_2\beta_2 M + \beta_3 M + \beta_4 M + d + \eta_2)\|V_3\|$$
$$+ \beta_3 M\|V_4\| + \beta_4 M\|V_5\| \leq C\sum_{i=1}^{5}\|V_i\|,$$

$$\|f_4(U_h) - f_4(\tilde{U}_h)\| \leq \alpha_3\beta_3 M\|V_3\| + (\alpha_3\beta_3 M + d + \eta_3)\|V_4\| \leq C\sum_{i=1}^{5}\|V_i\|,$$

$$\|f_5(U_h) - f_5(\tilde{U}_h)\| \leq \alpha_4\beta_4 M\|V_3\| + (\alpha_4\beta_4 M + d + \eta_4)\|V_5\| \leq C\sum_{i=1}^{5}\|V_i\|.$$

Therefore, from the above inequalities we have

$$\|f_i(U_h) - f_i(\tilde{U}_h)\| \leq C\sum_{i=1}^{5}\|V_i\|, \text{ for all } i \in \{1,\ldots,5\}. \tag{2.9}$$

Put (2.9) in (2.8), yields

$$\frac{1}{2}\frac{d}{dt}\|V_i\|^2 \leq C\sum_{i=1}^{5}\|V_i\|^2, \tag{2.10}$$

Integrating form 0 to t, we can reduce Equation (2.10) to

$$\|V_i(t)\|^2 \leq \|V_i(0)\|^2 + 2C\int_0^t\sum_{i=1}^{5}\|V_i(s)\|^2 ds. \tag{2.11}$$

Summing over components of (2.11), we have

$$\sum_{i=1}^{5}\|V_i(t)\|^2 \leq \sum_{i=1}^{5}\|V_i(0)\|^2 + 2C\int_0^t\sum_{i=1}^{5}\|V_i(s)\|^2 ds. \tag{2.12}$$

Applying Gronwall's inequality and $V_1(0) = \cdots = V_5(0) = 0$, we get:

$$\sum_{i=1}^{5}\|V_i(t)\|^2 \leq \sum_{i=1}^{5}\|V_i(0)\|^2 e^{2Ct} = 0. \tag{2.13}$$

We see that $V_i(t) = 0$, this means that $U_{i,h}(t) = \tilde{U}_{i,h}(t)$, for all $t \in [0,T]$ and for all $i = 1,\ldots,5$. □

2.2. **Error Analysis.** Now, we analyze the accuracy of the semi-discrete scheme (2.3). For all $u, v \in H_0^1$ satisfies the boundedness property

$$|(\frac{\partial u}{\partial x}, \frac{\partial v}{\partial x})| \leq M\|u\|_{H^1}\|v\|_{H^1}, \forall u, v \in H_0^1 \tag{2.14}$$

and coercivity property (on Ω)

$$(\frac{\partial v}{\partial x}, \frac{\partial v}{\partial x}) \geq \alpha\|v\|_{H^1}, \forall v \in H_0^1, \text{ for some } \alpha \in \mathbb{R}. \tag{2.15}$$

Also, satisfies

$$(\frac{\partial(v-\tilde{v})}{\partial x}, \frac{\partial w}{\partial x}) = 0, \ w \in S_h, \tag{2.16}$$

where $\tilde{v}$ is an auxiliary projection of v [2]. Now we have the following bound for error in the semi-discrete approximation.

Lemma 2.1.*[20] Assuming that a function u satisfies*

$$u \in L^\infty\big(H^r(\Omega)\big), \ \frac{\partial u}{\partial t} \in L^\infty\big(H^r(\Omega)\big),$$

then there holds the following inequalities:

$$\|\tilde{u} - u\| + h\,\|\nabla(\tilde{u} - u)\| \leq C_1 h^r \|u\|_r, \tag{2.17a}$$

$$\left\|\frac{\partial(\tilde{u}-u)}{\partial t}\right\| + h\left\|\nabla\left(\frac{\partial(\tilde{u}-u)}{\partial t}\right)\right\| \leq C_2 h^r \left\|\frac{\partial u}{\partial t}\right\|_r, \tag{2.17b}$$

where C_1 and C_2 are constants independent of h.

Theorem 2.2. *For the solutions $U_{1,h}, \ldots, U_{5,h} \in S_h$ of (2.3) and exact solutions $U_1, \ldots, U_5 \in H_0^r(\Omega)$ of (2.2), respectively, the error satisfies:*

$$\|U_{i,h} - U_i\| \leq Ch^r, \text{ for some } C > 0, \text{ and for all } i \in \{1, \ldots, 5\}.$$

Proof. For each component $i = 1, \ldots, 5$:

$$e_i = U_{h,i} - U_i = (U_{h,i} - R_h U_i) + (R_h U_i - U_i) = \theta_i + \rho_i,$$

where R_h is the Ritz projector. Using Lemma 2.1 for each component:

$$\|\rho_i\| + h\|\nabla\rho_i\| \leq C_1 h^r \|U_i\|_r, \tag{2.18}$$

$$\left\|\frac{\partial\rho_i}{\partial t}\right\| + h\left\|\nabla\frac{\partial\rho_i}{\partial t}\right\| \leq C_2 h^r \left\|\frac{\partial U_i}{\partial t}\right\|_r. \tag{2.19}$$

The error equation for component i is:

$$\left(\frac{\partial\theta_i}{\partial t}, w_h\right) + D_{H_i}(\nabla\theta_i, \nabla w_h) = -\left(\frac{\partial\rho_i}{\partial t}, w_h\right) + (f_i(U_h) - f_i(U), w_h). \tag{2.20}$$

Setting $w_h = \theta_i$ in (2.20), yields

$$\left(\frac{\partial\theta_i}{\partial t}, \theta_i\right) + D_{H_i}(\nabla\theta_i, \nabla\theta_i) = -\left(\frac{\partial\rho_i}{\partial t}, \theta_i\right) + (f_i(U_h) - f_i(U), \theta_i).$$

Using Lipschitz conditions defined in (2.9), along with Cauchy–Schwarz inequality, gives

$$\frac{1}{2}\frac{d}{dt}\|\theta_i\|^2 + D_{H_i}\|\nabla\theta_i\|^2 \leq \left\|\frac{\partial\rho_i}{\partial t}\right\|\|\theta_i\| + C\Big(\sum_{i=1}^{5}\|\theta_i + \rho_i\|\Big)\|\theta_i\|,$$

Apply Young's inequality, gives

$$\frac{d}{dt}\|\theta_i\|^2 + 2D_{H_i}\|\nabla\theta_i\|^2 \leq C\Big(\left\|\frac{\partial\rho_i}{\partial t}\right\|^2 + \sum_{i=1}^{5}\|\rho_i\|^2 + \sum_{i=1}^{5}\|\theta_i\|^2\Big),$$

Hence, we have

$$\frac{d}{dt}\|\theta_i\|^2 \leq C\Big(\Big\|\frac{\partial \rho_i}{\partial t}\Big\|^2 + \sum_{i=1}^{5}\|\rho_i\|^2 + \sum_{i=1}^{5}\|\theta_i\|^2\Big), \tag{2.21}$$

Summing over components of (2.21), we have

$$\sum_{i=1}^{5}\frac{d}{dt}\|\theta_i\|^2 \leq C\Big(\sum_{i=1}^{5}\Big\|\frac{\partial \rho_i}{\partial t}\Big\|^2 + \sum_{i=1}^{5}\|\rho_i\|^2 + \sum_{i=1}^{5}\|\theta_i\|^2\Big),$$

Integrating the last equation from 0 to t, gives

$$\sum_{i=1}^{5}\|\theta_i(t)\|^2 \leq \sum_{i=1}^{5}\|\theta_i(0)\|^2 + C\int_0^t\Big(\sum_{i=1}^{5}\Big(\Big\|\frac{\partial \rho_i(s)}{\partial t}\Big\|^2 + \|\rho_i(s)\|^2\Big) + \sum_{i=1}^{5}\|\theta_i(s)\|^2\Big)ds.$$

Set $\theta_1(0) = \cdots = \theta_5(0) = 0$, and using (2.18) and (2.19), we obtain

$$\sum_{i=1}^{5}\|\theta_i(t)\|^2 \leq Ch^{2r}\int_0^t\sum_{i=1}^{5}\|U_i(s)\|^2 ds + C\int_0^t\sum_{i=1}^{5}\|\theta_i(s)\|^2 ds.$$

Thus, we have

$$\sum_{i=1}^{5}\|\theta_i(t)\|^2 \leq Ch^{2r} + C\int_0^t\sum_{i=1}^{5}\|\theta(s)\|^2 ds.$$

Using Grownwall's lemma, we have the following

$$\sum_{i=1}^{5}\|\theta_i(t)\|^2 \leq Ch^{2r}e^{Ct} \leq Ce^{CT}h^{2r}.$$

Hence,

$$\|\theta_i(t)\|^2 \leq Ch^{2r}.$$

Thus,

$$\|\theta_i(t)\| \leq Ch^r. \tag{2.22}$$

So, from Equation (2.22) and by using Lemma 2.1, we have

$$\begin{aligned}\|U_{i,h} - U_i\| = \|\theta_i + \rho_i\| &\leq \|\theta_i\| + \|\rho_i\| \\ &\leq Ch^r + Ch^{r+1}\|U_i\|_{r+1} \\ &\leq Ch^r(1 + \|U_i\|_{r+1}) \\ &\leq C(U_i)h^r.\end{aligned}$$

Therefore, $\|U_{i,h} - U_i\| \leq Ch^r$, for all $i \in \{1, \ldots, 5\}$ □

3. Finite Element Formulation

In this section, we derive the finite element formulation corresponding to the given problem. To initiate the process, we begin by discretizing the spatial domain $[0, 2]$ into N uniform finite elements. Let $\{x_m\}_{m=0}^{N}$ be a partition of the interval $[0, 2]$ with $h = \frac{2}{N}$ and $x_m = mh$. The Lagrange function $\varphi_m(x)$ centered at node x_m is defined as:

$$\varphi_m(x) = \begin{cases}\frac{x - x_{m-1}}{h}, & \text{for } x_{m-1} \leq x \leq x_m, \\ \frac{x_{m+1} - x}{h}, & \text{for } x_m \leq x \leq x_{m+1}, \\ 0, & \text{otherwise.}\end{cases} \tag{3.1}$$

Using piecewise linear basis functions $\varphi_m(x)$, we approximate $\mathcal{H}, \mathcal{N}, \mathcal{Y}, \mathcal{V}$, and $\mathcal{Z}$ as:

$$\mathcal{H}(x,t) = \sum_{j=0}^{N} H_j(t)\varphi_j(x), \quad \mathcal{N}(x,t) = \sum_{j=0}^{N} N_j(t)\varphi_j(x), \quad \mathcal{Y}(x,t) = \sum_{j=0}^{N} Y_j(t)\varphi_j(x),$$
$$\mathcal{V}(x,t) = \sum_{j=0}^{N} V_j(t)\varphi_j(x), \quad \mathcal{Z}(x,t) = \sum_{j=0}^{N} Z_j(t)\varphi_j(x), \tag{3.2}$$

here $H_j(t), N_j(t), Y_j(t), V_j(t)$ and $Z_j(t)$'s are time dependent which are going to be determined. If we use local coordinate transformation $\xi = x - x_m$, $0 \le \xi \le h$, then we obtain the Lagrange basis functions as follows:

$$\begin{matrix}\varphi_{m-1} \\ \varphi_m\end{matrix} = \begin{cases}\frac{\xi}{h}, \\ \frac{h-\xi}{h},\end{cases} \qquad 0 \le \xi \le h. \tag{3.3}$$

By expressing the approximate solution (3.2) in terms of the local coordinate system, we obtain the following representation:

$$\mathcal{H}_n(\xi,t) = \sum_{j=m-1}^{m} H_j^e(t)\varphi_j^e(\xi), \quad \mathcal{N}_n(\xi,t) = \sum_{j=m-1}^{m} N_j^e(t)\varphi_j^e(\xi).$$
$$\mathcal{Y}_n(\xi,t) = \sum_{j=m-1}^{m} Y_j^e(t)\varphi_j^e(\xi), \quad \mathcal{V}_n(\xi,t) = \sum_{j=m-1}^{m} V_j^e(t)\varphi_j^e(\xi).$$
$$\mathcal{Z}_n(\xi,t) = \sum_{j=m-1}^{m} Z_j^e(t)\varphi_j^e(\xi). \tag{3.4}$$

Following straightforward manipulations, the weak formulation corresponding to Equation (3.2) is obtained as

$$\int_{x_m}^{x_{m+1}} \Big(\frac{\partial \mathcal{H}}{\partial t}w + D_{\mathcal{H}}\frac{\partial \mathcal{H}}{\partial x}\frac{\partial w}{\partial x} - \kappa w + d\mathcal{H}w + \beta_1 \mathcal{H}\,\mathcal{N}w + \beta_2 \mathcal{H}\mathcal{Y}w\Big)dx = 0 \tag{3.5a}$$
$$\int_{x_m}^{x_{m+1}} \Big(\frac{\partial \mathcal{N}}{\partial t}w + D_{\mathcal{N}}\frac{\partial \mathcal{N}}{\partial x}\frac{\partial w}{\partial x} - \alpha_1\beta_1 \mathcal{H}\,\mathcal{N}w + (d+\eta_1)\mathcal{N}w\Big)dx = 0 \tag{3.5b}$$
$$\int_{x_m}^{x_{m+1}} \Big(\frac{\partial \mathcal{Y}}{\partial t}w + D_{\mathcal{Y}}\frac{\partial \mathcal{Y}}{\partial x}\frac{\partial w}{\partial x} - \alpha_2\beta_2 \mathcal{H}\mathcal{Y}w + \beta_3 \mathcal{Y}\mathcal{V}w + \beta_4 \mathcal{Y}\mathcal{Z}w + (d+\eta_2)\mathcal{Y}w\Big)dx = 0 \tag{3.5c}$$
$$\int_{x_m}^{x_{m+1}} \Big(\frac{\partial \mathcal{V}}{\partial t}w + D_{\mathcal{V}}\frac{\partial \mathcal{V}}{\partial x}\frac{\partial w}{\partial x} - \mu w - \alpha_3\beta_3 \mathcal{Y}\mathcal{V}w + (d+\eta_3)\mathcal{V}w\Big)dx = 0 \tag{3.5d}$$
$$\int_{x_m}^{x_{m+1}} \Big(\frac{\partial \mathcal{Z}}{\partial t}w + D_{\mathcal{Z}}\frac{\partial \mathcal{Z}}{\partial x}\frac{\partial w}{\partial x} - \alpha_4\beta_4 \mathcal{Y}\mathcal{Z}w + (d+\eta_4)\mathcal{Z}w\Big)dx = 0 \tag{3.5e}$$

Since the Galerkin finite element method is employed in this study, the weight functions are selected to be the same as the basis functions, namely the Lagrange function. Substituting Equation (3.4) into Equation (3.5), we obtain the following

$$\sum_{j=m-1}^{m} \Big\{\Big(\int_0^h \varphi_i\varphi_j\, d\xi\Big)\dot{H}_j^e + D_{\mathcal{H}}\Big(\int_0^h \varphi_i'\varphi_j'\, d\xi\Big)H_j^e + d\Big(\int_0^h \varphi_i\varphi_j\, d\xi\Big)H_j^e$$
$$+ \beta_1 \sum_{k=m-1}^{m}\Big(\int_0^h \varphi_i\varphi_j\varphi_k\, d\xi\Big)H_k^e N_j^e + \beta_2 \sum_{k=m-1}^{m}\Big(\int_0^h \varphi_i\varphi_j\varphi_k\, d\xi\Big)H_k^e Y_j^e\Big\}$$
$$- \kappa\Big(\int_0^h \varphi_i\, d\xi\Big) = 0, \tag{3.6a}$$

$$\sum_{j=m-1}^{m}\Big\{\Big(\int_0^h \varphi_i\varphi_j\ d\xi\Big)\dot{N}_j^e + D_{\mathcal{N}}\Big(\int_0^h \varphi_i'\varphi_j'\ d\xi\Big)N_j^e - \alpha_1\beta_1\sum_{k=m-1}^{m}\Big(\int_0^h \varphi_i\varphi_j\varphi_k\ d\xi\Big)H_k^eN_j^e$$
$$+ (d+\eta_1)\Big(\int_0^h \varphi_i\varphi_j\ d\xi\Big)N_j^e\Big\} = 0, \tag{3.6b}$$
$$\sum_{j=m-1}^{m}\Big\{\Big(\int_0^h \varphi_i\varphi_j\ d\xi\Big)\dot{Y}_j^e + D_{\mathcal{Y}}\Big(\int_0^h \varphi_i'\varphi_j'\ d\xi\Big)Y_j^e - \alpha_2\beta_2\sum_{k=m-1}^{m}\Big(\int_0^h \varphi_i\varphi_j\varphi_k\ d\xi\Big)H_k^eY_j^e$$
$$+ \beta_3\sum_{k=m-1}^{m}\Big(\int_0^h \varphi_i\varphi_j\varphi_k\ d\xi\Big)Y_k^eV_j^e + \beta_4\sum_{k=m-1}^{m}\Big(\int_0^h \varphi_i\varphi_j\varphi_k\ d\xi\Big)Y_k^eZ_j^e$$
$$+ (d+\eta_2)\Big(\int_0^h \varphi_i\varphi_j\ d\xi\Big)Y_j^e\Big\} = 0, \tag{3.6c}$$
$$\sum_{j=m-1}^{m}\Big\{\Big(\int_0^h \varphi_i\varphi_j\ d\xi\Big)\dot{V}_j^e + D_{\mathcal{V}}\Big(\int_0^h \varphi_i'\varphi_j'\ d\xi\Big)V_j^e - \alpha_3\beta_3\sum_{k=m-1}^{m}\Big(\int_0^h \varphi_i\varphi_j\varphi_k\ d\xi\Big)Y_k^eV_j^e$$
$$+ (d+\eta_3)\Big(\int_0^h \varphi_i\varphi_j\ d\xi\Big)V_j^e\Big\} - \mu\Big(\int_0^h \varphi_i\ d\xi\Big) = 0, \tag{3.6d}$$
$$\sum_{j=m-1}^{m}\Big\{\Big(\int_0^h \varphi_i\varphi_j\ d\xi\Big)\dot{Z}_j^e + D_{\mathcal{Z}}\Big(\int_0^h \varphi_i'\varphi_j'\ d\xi\Big)Z_j^e - \alpha_4\beta_4\sum_{k=m-1}^{m}\Big(\int_0^h \varphi_i\varphi_j\varphi_k\ d\xi\Big)Y_k^eZ_j^e$$
$$+ (d+\eta_4)\Big(\int_0^h \varphi_i\varphi_j\ d\xi\Big)Z_j^e\Big\} = 0, \tag{3.6e}$$

Upon rearranging this system into its matrix form, we arrive at the following representation:

$$M^e\dot{H}^e + D_{\mathcal{H}}A^eH^e + dM^eH^e + \beta_1F^e(H^e)N^e + \beta_2F^e(H^e)Y^e - \kappa B^e = 0, \tag{3.7a}$$
$$M^e\dot{N}^e + D_{\mathcal{N}}A^eN^e - \alpha_1\beta_1F^e(H^e)N^e + (d+\eta_1)M^eN^e = 0, \tag{3.7b}$$
$$M^e\dot{Y}^e + D_{\mathcal{Y}}A^eY^e - \alpha_2\beta_2F^e(H^e)Y^e + \beta_3F^e(Y^e)V^e + \beta_4F^e(Y^e)Z^e + (d+\eta_2)M^eY^e = 0, \tag{3.7c}$$
$$M^e\dot{V}^e + D_{\mathcal{V}}A^eV^e - \alpha_3\beta_3F^e(Y^e)V^e + (d+\eta_3)M^eV^e - \mu B^e = 0, \tag{3.7d}$$
$$M^e\dot{Z}^e + D_{\mathcal{Z}}A^eZ^e - \alpha_4\beta_4F^e(Y^e)Z^e + (d+\eta_4)M^eZ^e = 0, \tag{3.7e}$$

here the dot symbol denotes differentiation with respect to t, and the vectors $H^e = \big(H_{m-1}^e, H_m^e\big)$, $N^e = \big(N_{m-1}^e, N_m^e\big)$, $Y^e = \big(Y_{m-1}^e, Y_m^e\big)$, $V^e = \big(V_{m-1}^e, V_m^e\big)$, and $Z^e = \big(Z_{m-1}^e, Z_m^e\big)$ are treated as the local (element-wise) nodal parameter vectors. The element matrices $M^e, A^e, F^e(\alpha)$ and B^e are defined through the following integrals:

$$M_{ij}^e = \int_0^h \varphi_i\varphi_j\ d\xi,$$
$$A_{ij}^e = \int_0^h \varphi_i'\varphi_j'\ d\xi, \tag{3.8}$$
$$F_{ijk}^e = \int_0^h \varphi_i\varphi_j\varphi_k\ d\xi.$$
$$B_i^e = \int_0^h \varphi_i\ d\xi.$$

where $i, j, k = m-1, m$. The element matrices introduced in Equation (3.8) can be explicitly computed using the following expressions:

$$M^e = \frac{h}{6}\begin{bmatrix} 2 & 1 \\ 1 & 2 \end{bmatrix}, \tag{3.9}$$

$$A^e = \frac{1}{h}\begin{bmatrix} 1 & -1 \\ -1 & 1 \end{bmatrix}, \tag{3.10}$$

$$F^e(H^e) = \frac{h}{12}\begin{bmatrix} (3,1)H^e & (1,1)H^e \\ (1,1)H^e & (1,3)H^e \end{bmatrix}, \tag{3.11}$$

$$F^e(Y^e) = \frac{h}{12}\begin{bmatrix} (3,1)Y^e & (1,1)Y^e \\ (1,1)Y^e & (1,3)Y^e \end{bmatrix}, \tag{3.12}$$

$$B^e = \frac{h}{2}\begin{bmatrix} 1 \\ 1 \end{bmatrix}. \tag{3.13}$$

By assembling the contributions of all elements over the entire solution domain, the following system of ordinary differential equations is obtained:

$$\dot{H} = -M^{-1}\Big(D_{\mathcal{H}}AH + dMH + \beta_1 F(H)N + \beta_2 F(H)Y - \kappa B\Big), \tag{3.14a}$$

$$\dot{N} = -M^{-1}\Big(D_{\mathcal{N}}AN - \alpha_1\beta_1 F(H)N + (d+\eta_1)MN\Big), \tag{3.14b}$$

$$\dot{Y} = -M^{-1}\Big(D_{\mathcal{Y}}AY - \alpha_2\beta_2 F(H)Y + \beta_3 F(Y)V + \beta_4 F(Y)Z + (d+\eta_2)MY\Big), \tag{3.14c}$$

$$\dot{V} = -M^{-1}\Big(D_{\mathcal{V}}AV - \alpha_3\beta_3 F(Y)V + (d+\eta_3)MV - \mu B\Big), \tag{3.14d}$$

$$\dot{Z} = -M^{-1}\Big(D_{\mathcal{Z}}AZ - \alpha_4\beta_4 F(Y)Z + (d+\eta_4)MZ\Big), \tag{3.14e}$$

where the global element parameter vectors are defined as $\delta = (\delta_0, \delta_1, \ldots, \delta_N)$ where M, A, and $F(\delta)$ represent the global element matrices and δ represents each of H, N, Y, V and Z. The generalized m^{th} row of these global matrices can be expressed as follows:

$$M : \frac{h}{6}(1,4,1), \tag{3.15}$$

$$A : \frac{1}{h}(-1,2,-1), \tag{3.16}$$

$$F(H) : \frac{h}{12}((1,1,0)H^m, (1,6,1)H^m, (0,1,1)H^m), \tag{3.17}$$

$$F(Y) : \frac{h}{12}((1,1,0)Y^m, (1,6,1)Y^m, (0,1,1)Y^m). \tag{3.18}$$

By using the Euler method for $\dot{\delta} = \dfrac{\delta^{n+1} - \delta^n}{\Delta t}$, where Δt is the step size of time discretization. After simplification Equation (3.14) reduces to:

$$H^{n+1} = H^n - \Delta t M^{-1}\Big(D_{\mathcal{H}}AH^n + dMH^n + \beta_1 F(H^n)N^n + \beta_2 F(H^n)Y^n - \kappa B\Big), \tag{3.19a}$$

$$N^{n+1} = N^n - \Delta t M^{-1}\Big(D_{\mathcal{N}}AN^n - \alpha_1\beta_1 F(H^n)N^n + (d+\eta_1)MN^n\Big), \tag{3.19b}$$

$$Y^{n+1} = Y^n - \Delta t M^{-1}\Big(D_{\mathcal{Y}}AY^n - \alpha_2\beta_2 F(H^n)Y^n + \beta_3 F(Y^n)V^n + \beta_4 F(Y^n)Z^n + (d+\eta_2)MY^n\Big), \tag{3.19c}$$

$$V^{n+1} = V^n - \Delta t M^{-1}\Big(D_{\mathcal{V}}AV^n - \alpha_3\beta_3 F(Y^n)V^n + (d+\eta_3)MV^n - \mu B\Big), \tag{3.19d}$$

$$Z^{n+1} = Z^n - \Delta t M^{-1}\Big(D_{\mathcal{Z}}AZ^n - \alpha_4\beta_4 F(Y^n)Z^n + (d+\eta_4)MZ^n\Big), \tag{3.19e}$$

TABLE 2. Model parameters and their biological interpretations

Symbol	Parameter	Value	Units
p_1	κ	0.02	nutrient·day^{-1}
p_2	μ	0.01	virus·day^{-1}
p_3	d	0.02	day^{-1}
p_4	α_1	0.8	dimensionless
p_5	α_2	0.8	dimensionless
p_6	α_3	0.5	dimensionless
p_7	α_4	0.8	dimensionless
p_8	β_1	0.03	(nutrient·cell)$^{-1}$·day^{-1}
p_9	β_2	0.03	(nutrient·cell)$^{-1}$·day^{-1}
p_{10}	β_3	0.1	(virus·cell)$^{-1}$·day^{-1}
p_{11}	β_4	0.03	(CTL·cell)$^{-1}$·day^{-1}
p_{12}	η_1	0.04	day^{-1}
p_{13}	η_2	0.01	day^{-1}
p_{14}	η_3	0.008	day^{-1}
p_{15}	η_4	0.01	day^{-1}
p_{16}	$D_{\mathcal{H}}$	0.01	nutrient·day^{-1}·cell^{-1}
p_{17}	$D_{\mathcal{N}}$	0.01	cell·day^{-1}
p_{18}	$D_{\mathcal{Y}}$	0.03	cell·day^{-1}
p_{19}	$D_{\mathcal{V}}$	0.03	virus·day^{-1}
p_{20}	$D_{\mathcal{Z}}$	0.03	CTL·day^{-1}

In order to start the solution procedure described in Equation (3.19), the initial vector H^0, M^0, Y^0, V^0, and Z^0 must first be determined from the initial condition. Once the parameter H^{n+1}, M^{n+1}, Y^{n+1}, V^{n+1}, and Z^{n+1} have been computed iteratively in terms of the parameter H^n, M^n, Y^n, V^n, and Z^n at time t, the solution at each nodal point can then be evaluated using the expression $\mathcal{H}(x_i,t) = H_i$, $\mathcal{M}(x_i,t) = M_i$, $\mathcal{Y}(x_i,t) = Y_i$, $\mathcal{V}(x_i,t) = V_i$, and $\mathcal{Z}(x_i,t) = Z_i$.

4. Sensitivity Analysis

In mathematical biology, sensitivity analysis serves as a fundamental tool for understanding how parameter variations influence therapeutic outcomes in oncolytic virotherapy. We present a comprehensive framework combining non-normalized, half-normalized, and fully normalized sensitivity measures tailored to our reaction-diffusion model of tumor-virus-immune interactions (1.1). Consider the system with five biological components $\mathbf{U} = (U_1, \ldots, U_5) = (\mathcal{H}, \mathcal{N}, \mathcal{Y}, \mathcal{V}, \mathcal{Z})$
The local sensitivity matrix $\mathbf{S}(\mathbf{x},t) \in \mathbb{R}^{5\times 20}$ quantifies how the component U_i responds to parameter p_j, where $\mathbf{p} = (p_1, ..., p_{20})$ is defined in Table 2:
We implement three complementary sensitivity measures:
Non-Normalized Sensitivity: The absolute sensitivity measures raw parameter influence:

$$S_{ij}^{\text{abs}} = \frac{\partial U_i}{\partial p_j}. \tag{4.1}$$

Particularly important for determining therapeutic dose-response relationships, and identifying critical thresholds for tumor eradication.
Half-Normalized Sensitivity: The state-scaled sensitivity accounts for component magnitudes:

$$S_{ij}^{\text{half}} = \frac{1}{U_i}\frac{\partial U_i}{\partial p_j}. \tag{4.2}$$

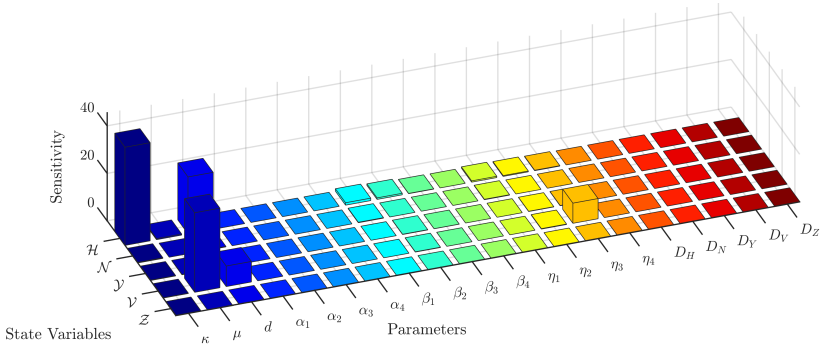

FIGURE 1. For the model (1.1), local sensitivity analysis is performed using the non-normalization approach provided in Equation (4.1).

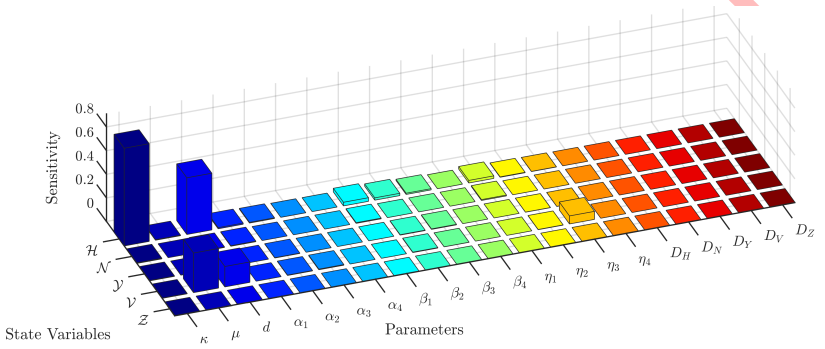

FIGURE 2. For the model (1.1), local sensitivity analysis is performed using the half-normalization approach provided in Equation (4.2).

Advantages include dimensionless comparison across different tumor microenvironments, and identification of relative vulnerabilities in tumor subpopulations.

Fully Normalized Sensitivity: The elasticity coefficient provides scale-invariant measurement:

$$S_{ij}^{\text{full}} = \frac{p_j}{U_i}\frac{\partial U_i}{\partial p_j}. \tag{4.3}$$

The concept of local sensitivity analysis is applied to our proposed oncolytic M1 virotherapy model. The initial concentrations of biological components and system parameters are defined in Table 2. Through comprehensive sensitivity analysis, we examine how variations in these parameters influence the temporal dynamics of tumor-virus-immune interactions.

To reveal the parameter impacts on system (1.1), local sensitivity analysis will carry out with non-normalized, fully normalized and half-normalized methods, respectively, which are shown in Figures 1, 2, and 3. These methods make evident different features of parameter importance with respect to each of the state variables.

The non-normalized sensitivity analysis (Figure 1) depicts the state variable behavior for parameters. The nutrient concentration ($\mathcal{H}$) displays a remarkably high sensitivity index of 41.46 for the nutrient supply rate (κ), whereas the tumor cells ($\mathcal{Y}$) are moderately sensitive to the growth rate parameters (α_2, β_2) with values of 0.14 and 0.39, respectively. Importantly, the immune response ($\mathcal{Z}$) is highly sensitive to the decay rate (η_4) with a sensitivity index of 37.05, underlining the importance of the decay rate parameter in a non-normalized fashion. The viral population ($\mathcal{V}$) is highly sensitive to the viral replication rate (μ) with a sensitivity index of 33.50, which underlines its importance in the unnormalized system dynamics.

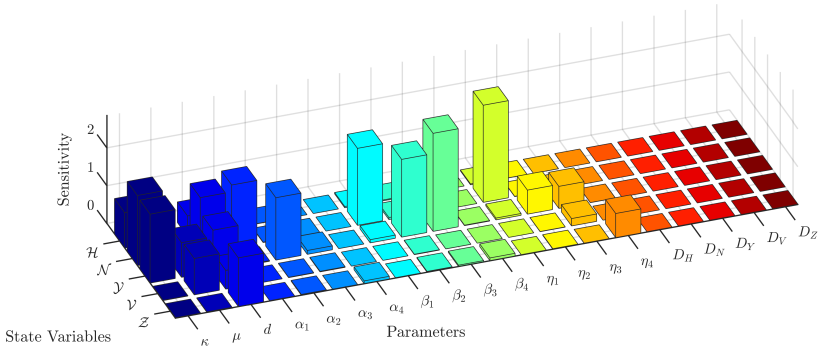

FIGURE 3. For the model (1.1), local sensitivity analysis is performed using the fully-normalization approach provided in Equation (4.3).

In the half-normalized analysis (Figure 2), relative sensitivities become more balanced. The normal cell population ($\mathcal{N}$) shows reduced but still significant sensitivity (0.0049-0.0053) to parameters related to nutrients (α_1, β_1), while tumor cells ($\mathcal{Y}$) maintain sensitivity (0.0028-0.0032) to viral infection rates (β_3). The viruses ($\mathcal{V}$) retain a strong dependence (0.34) on their replication rate (μ), though less extreme than in the raw analysis. Immune cells ($\mathcal{Z}$) now show a comparable sensitivity (0.00037) to both viral lysis (β_4) and immune decay (η_4), indicating the balanced importance of these parameters when partial normalization is applied.

The fully normalized results (Figure 3) provide the most nuanced information. The normal cell population ($\mathcal{N}$) is most sensitive to η_1 with sensitivity index 2.51. Tumor cells ($\mathcal{Y}$) are more sensitive (1.59-2.49) to both nutrient uptake (β_2) and viral infection (β_3), while viruses ($\mathcal{V}$) show a strong dependence (0.97) on their intrinsic replication (μ). In particular, the immune response ($\mathcal{Z}$) demonstrates dual sensitivity (0.63-0.66) to both its activation (β_4) and decay (η_4), revealing a critical balance in immunotherapeutic effects. Nutrient dynamics ($\mathcal{H}$) remain more sensitive (0.94) to supply rate (κ), but with reduced dominance compared to other variables. These results collectively identify β_2, β_3, and μ as the most influential parameters when the parameters and state variable scales are taken into account. Note that all three sensitivity analyses include the diffusion coefficients ($D_{\mathcal{H}}$, $D_{\mathcal{N}}$, $D_{\mathcal{Y}}$, $D_{\mathcal{V}}$, $D_{\mathcal{Z}}$), allowing us to assess the importance of spatial transport mechanisms alongside the kinetic parameters in our reaction-diffusion model.

5. Numerical Implementation

The nonlinear nature of the equation system (1.1) precludes the existence of analytical solutions in current research. To examine the spatiotemporal behavior of the M1 oncolytic virotherapy model described by equations (1.1). Our spatial domain spans the interval [0,2], utilizing a grid spacing of $\Delta x = 0.1$ and time increment $\Delta t = 0.001$. The following parameter values, consistent with those used in [8, 19], are employed: $\kappa = 0.02$, $\mu = 0.01$, $d = 0.02$, $\alpha_1 = 0.8$, $\alpha_3 = 0.5$, $\alpha_4 = 0.8$, $D_H = D_N = D_Y = 0.01$, $D_V = D_Z = 0.03$. The remaining parameters are treated as free variables, determined later.

The initial conditions for all model components are given by periodic functions with amplitude modulation [4]:

$$\phi_1(x) = 0.3(1 + 0.2\cos^2 \pi x), \quad \phi_2(x) = 0.2(1 + 0.2\cos^2 \pi x), \quad \phi_3(x) = 0.1(1 + 0.2\cos^2 \pi x),$$
$$\phi_4(x) = 0.1(1 + 0.2\cos^2 \pi x), \quad \phi_5(x) = 0.01(1 + 0.2\cos^2 \pi x).$$

Numerical convergence is rigorously verified through systematic grid refinement studies. For each model component $\zeta \in \{\mathcal{H}, \mathcal{N}, \mathcal{Y}, \mathcal{V}, \mathcal{Z}\}$, we compute successive solution differences:

$$E\zeta_1 = |\zeta(x,t)_{\Delta t=0.1, m=20} - \zeta(x,t)_{\Delta t=0.05, m=30}|$$
$$E\zeta_2 = |\zeta(x,t)_{\Delta t=0.05, m=30} - \zeta(x,t)_{\Delta t=0.01, m=40}|$$
$$E\zeta_3 = |\zeta(x,t)_{\Delta t=0.01, m=40} - \zeta(x,t)_{\Delta t=0.005, m=50}|$$

where m denotes the spatial discretization parameter.

TABLE 3. Absolute differences between successive numerical solutions of system (3.19) at $t = 10$ for $(\Delta t, m) = (0.1, 20)$ vs $(0.05, 30)$, $(0.05, 30)$ vs $(0.01, 40)$, and $(0.01, 40)$ vs $(0.005, 50)$. Parameter values are $\beta_1 = 0.03$, $\beta_2 = 0.03$, $\beta_3 = 0.1$, $\beta_4 = 0.03$, $\eta_1 = 0.04$, $\eta_2 = 0.01$, $\eta_3 = 0.008$, $\eta_4 = 0.01$, $\alpha_2 = 0.8$.

x	0.0	0.4	0.8	1.2	1.6	2.0
$E\mathcal{H}_1 \times 10^5$	2.65	111.39	181.60	181.60	111.39	2.65
$E\mathcal{H}_2 \times 10^5$	2.12	31.81	52.75	52.75	31.81	2.12
$E\mathcal{H}_3 \times 10^5$	0.26	9.38	15.34	15.34	9.38	0.26
$E\mathcal{N}_1 \times 10^5$	9.92	81.16	125.01	125.01	81.16	9.92
$E\mathcal{N}_2 \times 10^5$	7.92	29.08	42.13	42.13	29.08	7.92
$E\mathcal{N}_3 \times 10^5$	0.99	7.00	10.71	10.71	7.00	0.99
$E\mathcal{Y}_1 \times 10^5$	1.96	3.10	3.80	3.80	3.10	1.96
$E\mathcal{Y}_2 \times 10^5$	1.56	1.69	1.77	1.77	1.69	1.56
$E\mathcal{Y}_3 \times 10^5$	0.20	0.22	0.23	0.23	0.22	0.20
$E\mathcal{V}_1 \times 10^5$	3.84	3.10	2.65	2.65	3.10	3.84
$E\mathcal{V}_2 \times 10^5$	3.07	3.05	3.04	3.04	3.05	3.07
$E\mathcal{V}_3 \times 10^5$	0.38	0.38	0.38	0.38	0.38	0.38
$E\mathcal{Z}_1 \times 10^5$	0.16	0.22	0.26	0.26	0.22	0.16
$E\mathcal{Z}_2 \times 10^5$	0.12	0.13	0.13	0.13	0.13	0.12
$E\mathcal{Z}_3 \times 10^5$	0.02	0.02	0.02	0.02	0.02	0.02

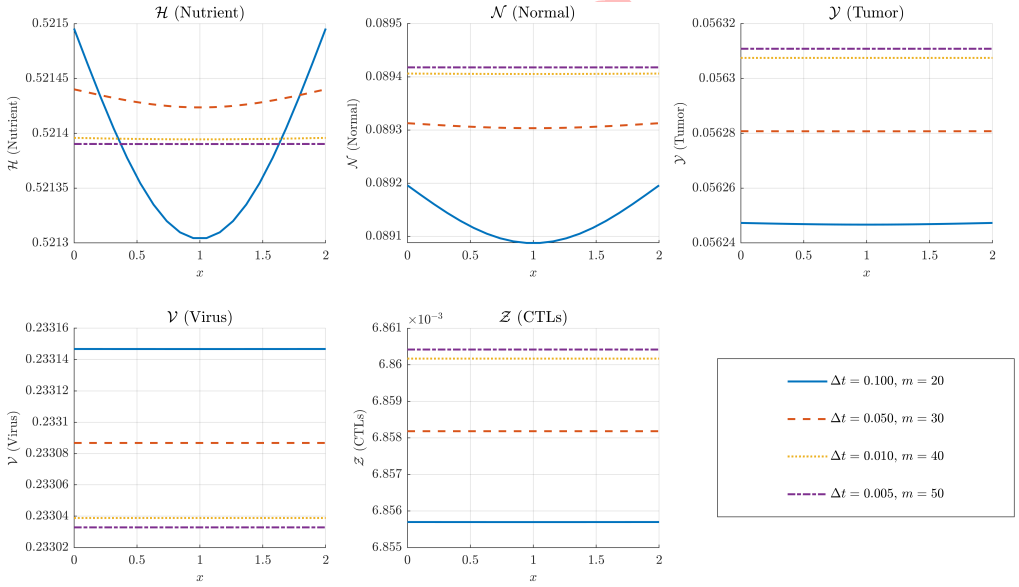

FIGURE 4. Comparing numerical solutions of system (3.19) at $t = 20$, for different Δt and m values, where the value of parameters are defined as in Table 3.

Figures 5 and 7, and Table 3 demonstrate that the absolute difference between the computed solutions progressively decreases as the mesh is refined, indicating the convergence of the numerical method.

Figure 8 demonstrates that in the absence of immune response, although tumor eradication is achieved, normal cell recovery fails, ultimately resulting in patient mortality.

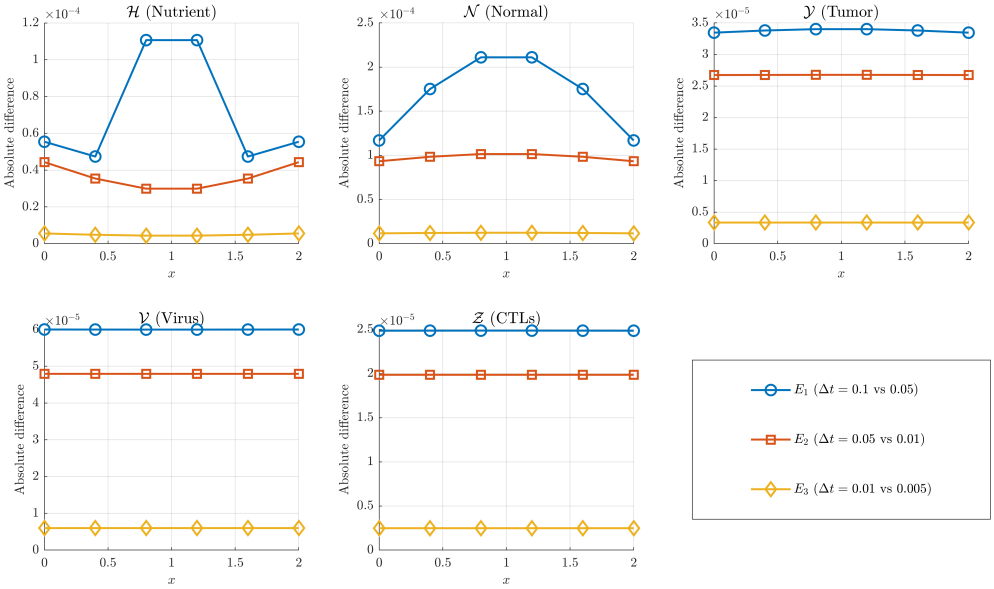

FIGURE 5. Absolute differences for numerical solutions of system (3.19) at $t = 20$, where the value of parameters are defined as in Table 3.

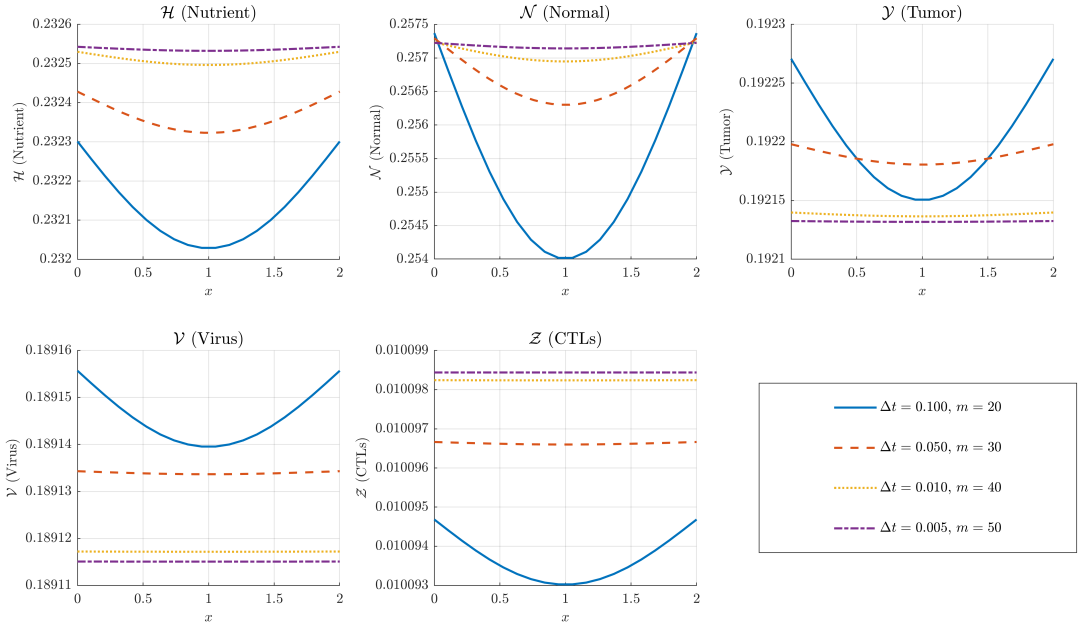

FIGURE 6. Comparing numerical solutions of system (3.19) at $t = 20$, for different Δt and m values, where the value of parameters are $\beta_1 = 0.15$, $\beta_2 = 0.5$, $\beta_3 = 0.05$, $\beta_4 = 0.6$, $\eta_1 = 0.008$, $\eta_2 = 0.008$, $\eta_3 = 0.005$, $\eta_4 = 0.02$, $\alpha_2 = 0.9$.

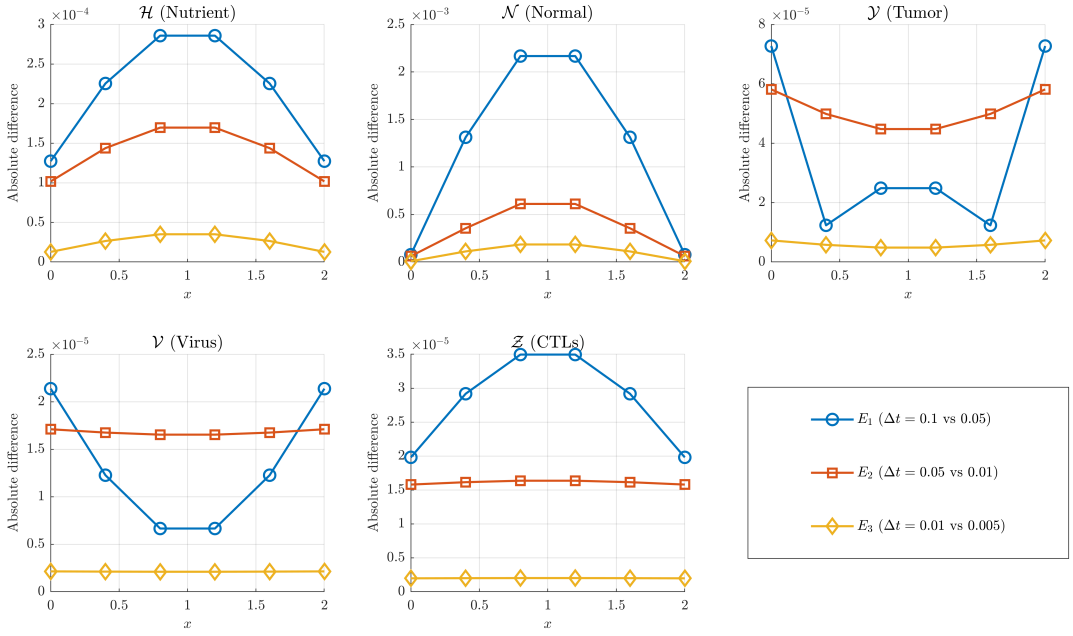

FIGURE 7. Absolute differences for numerical solutions of system (3.19) at $t = 20$, where the value of parameters are defined as in Figure 6.

Figure 9 indicates that M1 virotherapy alone depletes normal cells without successfully eliminating tumors, thereby posing a severe health risk.

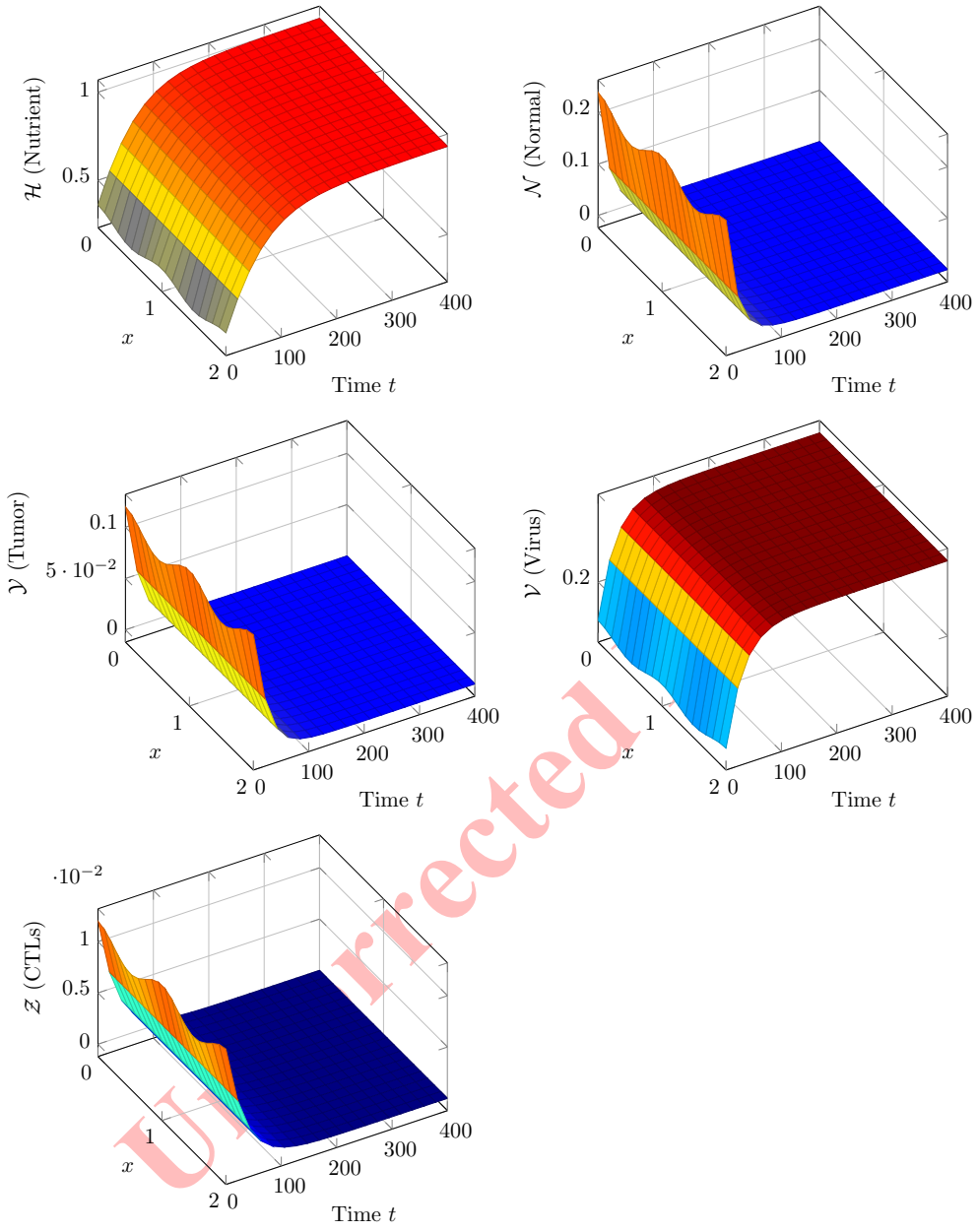

FIGURE 8. Numerical solution for the proposed model (1), where the value of parameters are $\beta_1 = 0.03$, $\beta_2 = 0.03$, $\beta_3 = 0.1$, $\beta_4 = 0.03$, $\eta_1 = 0.04$, $\eta_2 = 0.01$, $\eta_3 = 0.008$, $\eta_4 = 0.01$, $\alpha_2 = 0.8$.

In contrast, Figure 10 shows that tumor clearance and normal cell restoration are possible even without immune engagement, leading to an improvement in patient condition.

Figure 11 reveals that while anti-tumor immune activity suppresses tumor growth, it also significantly reduces viral concentration, resulting in treatment failure.

Figure 12 represents a partially effective strategy, where M1 viruses lower tumor burden and enhance normal cell populations in the absence of immune response, yet do not achieve complete tumor elimination.

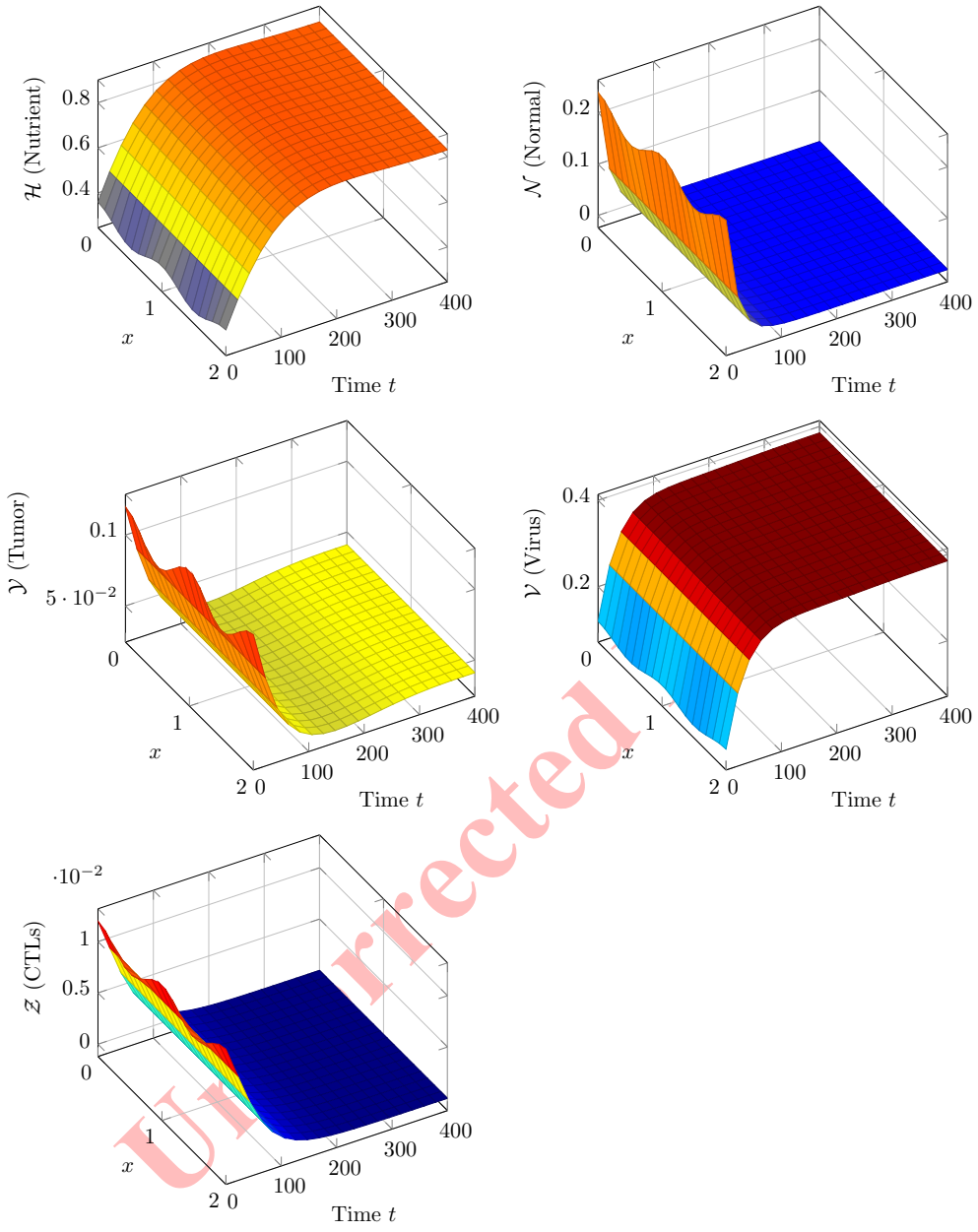

FIGURE 9. Numerical solution for the proposed model (1), where the value of parameters are $\beta_1 = 0.03$, $\beta_2 = 0.1$, $\beta_3 = 0.1$, $\beta_4 = 0.2$, $\eta_1 = 0.04$, $\eta_2 = 0.008$, $\eta_3 = 0.008$, $\eta_4 = 0.01$, $\alpha_2 = 0.8$.

Finally, Figure 13 highlights that reduced viral load diminishes therapeutic efficacy. Although immune responses constrain tumor progression, they fall short of ensuring complete tumor removal.

The computational experiments encompass six distinct biological scenarios as show in Figure 8–13. The numerical solutions exhibit consistent convergence under mesh refinement, as demonstrated by decreasing error between successive approximations. This systematic reduction in numerical error, typically following a power-law relationship with grid spacing, validates the stability and convergence properties of our discretization scheme.

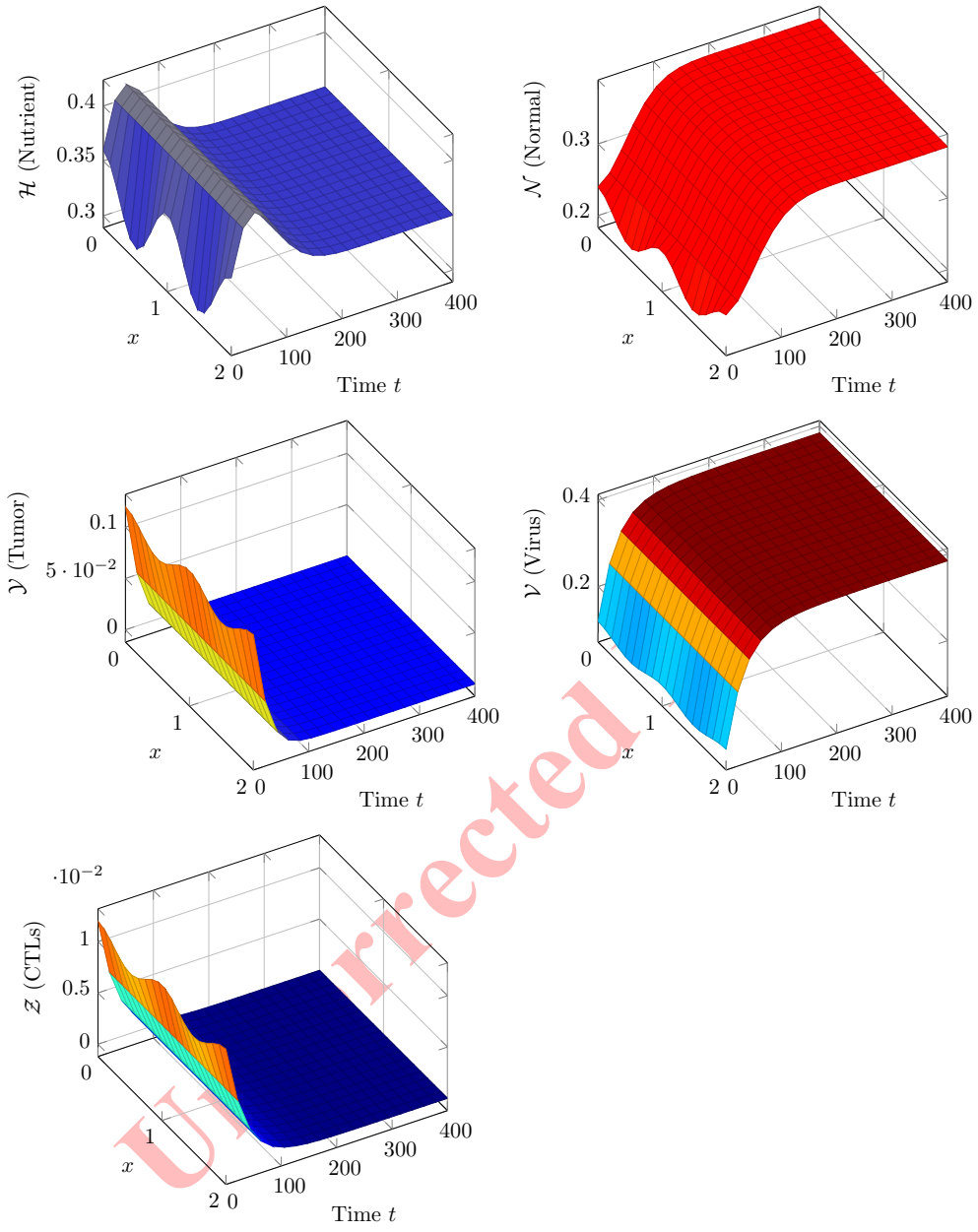

FIGURE 10. Numerical solution for the proposed model (1), where the value of parameters are $\beta_1 = 0.1$, $\beta_2 = 0.03$, $\beta_3 = 0.1$, $\beta_4 = 0.03$, $\eta_1 = 0.008$, $\eta_2 = 0.01$, $\eta_3 = 0.006$, $\eta_4 = 0.01$, $\alpha_2 = 0.8$.

The inclusion of diffusive transport mechanisms yields nontrivial spatiotemporal patterning. Key findings include: Nutrient concentrations exhibit positive correlation with the parameter β_4, Neoplastic cell populations demonstrate exponential temporal decay, and free M1 viral particle dynamics follow biphasic kinetics consistent with prior in vitro studies. The emergent spatial patterns provide novel insights into the complex nonlinear dynamics governing cancer-virotherapy interactions, particularly regarding the role of diffusion-limited transport in therapeutic efficacy. Results align with reference [4], demonstrating accurate solutions in all parameter configurations.

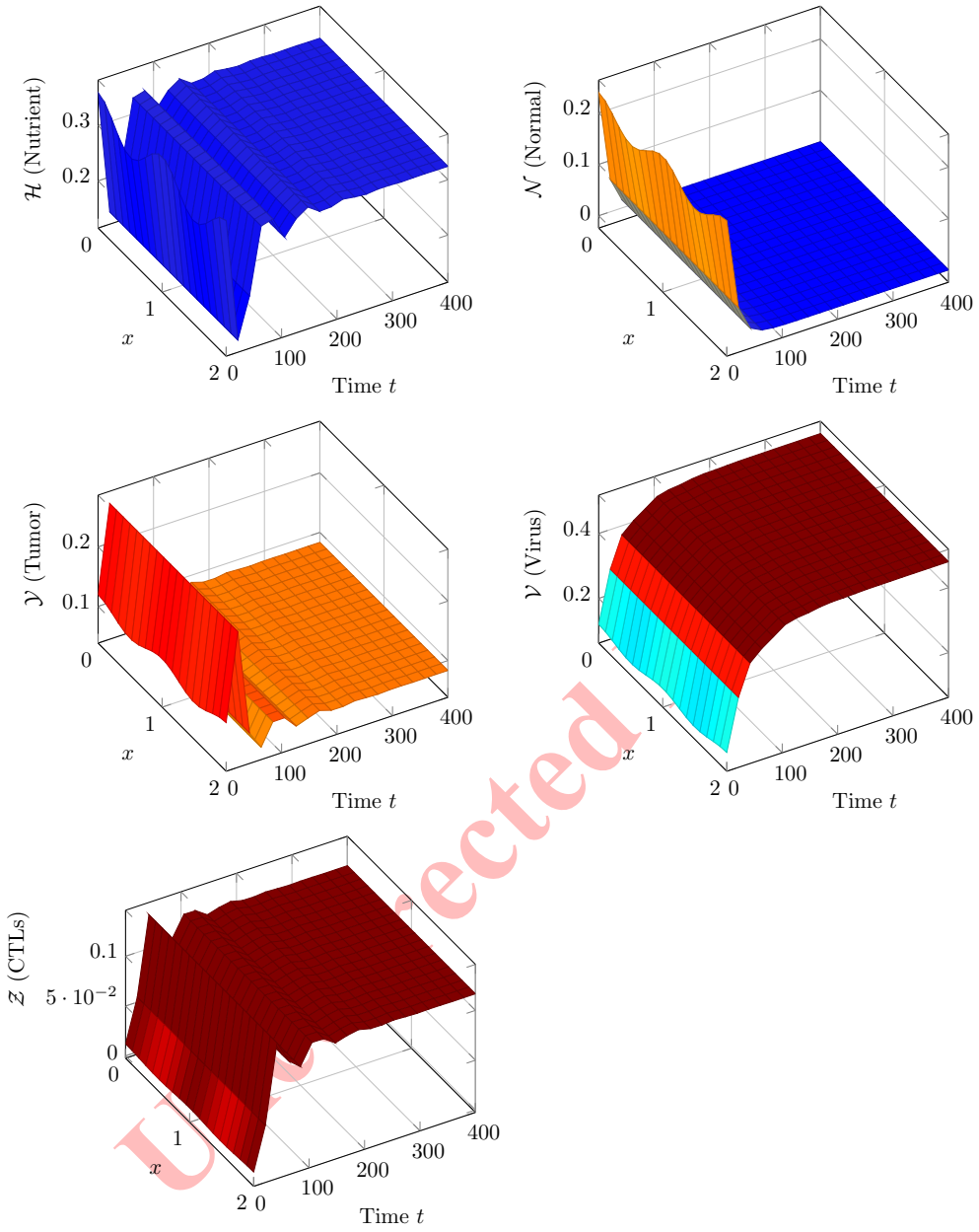

FIGURE 11. Numerical solution for the proposed model (1), where the value of parameters are $\beta_1 = 0.04$, $\beta_2 = 0.5$, $\beta_3 = 0.1$, $\beta_4 = 0.6$, $\eta_1 = 0.05$, $\eta_2 = 0.008$, $\eta_3 = 0.005$, $\eta_4 = 0.02$, $\alpha_2 = 0.9$.

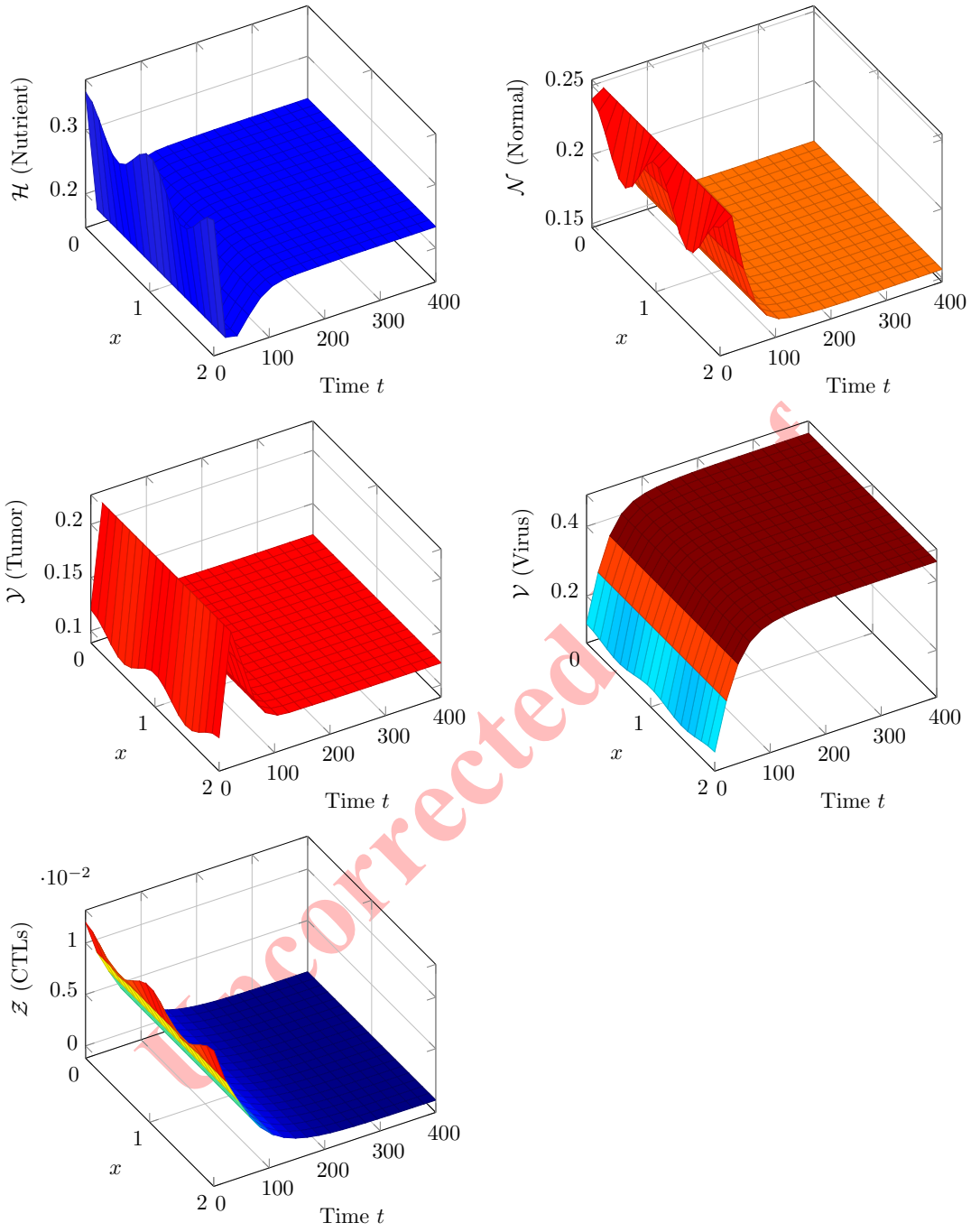

FIGURE 12. Numerical solution for the proposed model (1), where the value of parameters are $\beta_1 = 0.15$, $\beta_2 = 0.35$, $\beta_3 = 0.1$, $\beta_4 = 0.1$, $\eta_1 = 0.008$, $\eta_2 = 0.008$, $\eta_3 = 0.008$, $\eta_4 = 0.01$, $\alpha_2 = 0.9$.

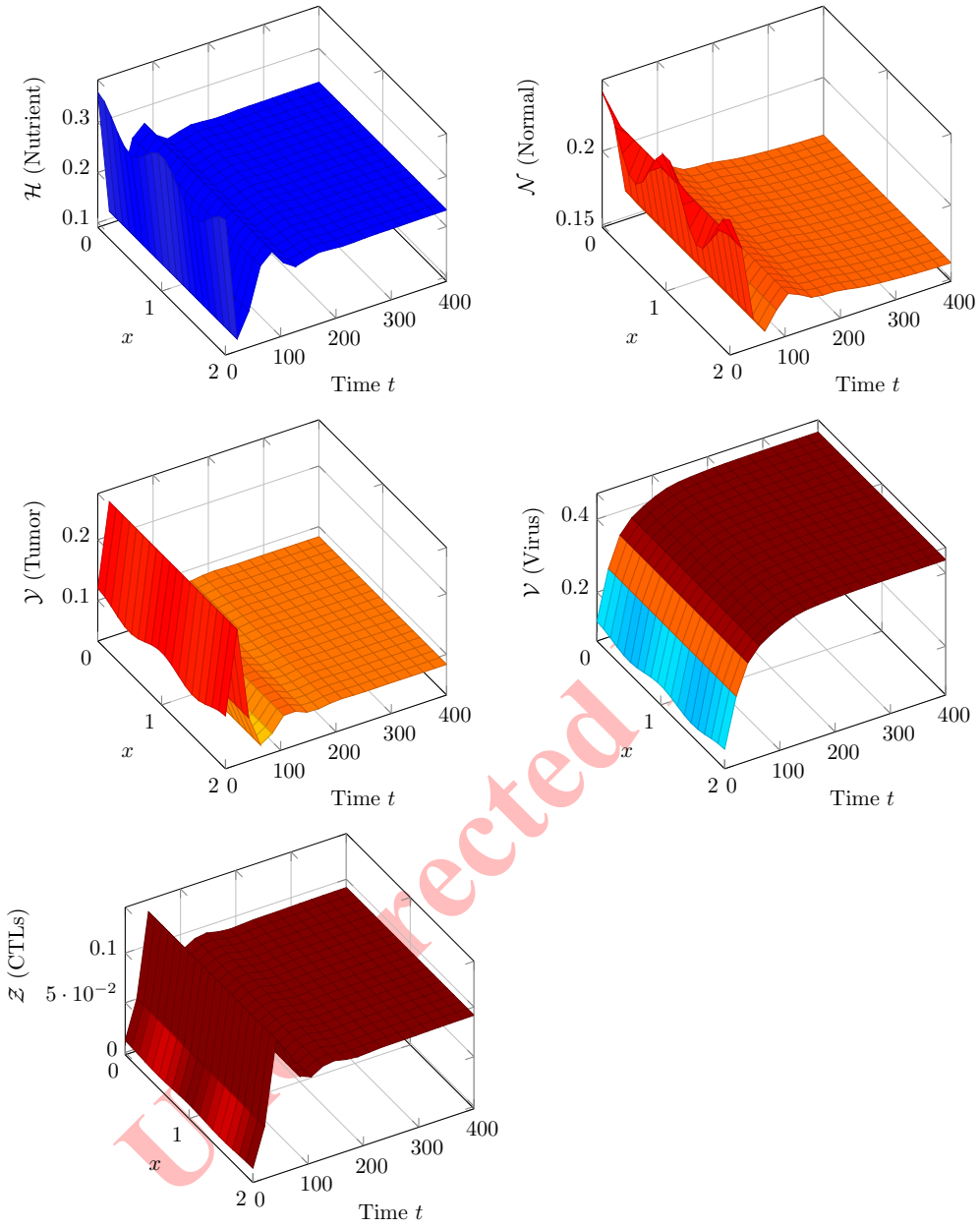

FIGURE 13. Numerical solution for the proposed model (1), where the value of parameters are $\beta_1 = 0.15$, $\beta_2 = 0.5$, $\beta_3 = 0.05$, $\beta_4 = 0.6$, $\eta_1 = 0.008$, $\eta_2 = 0.008$, $\eta_3 = 0.005$, $\eta_4 = 0.02$, $\alpha_2 = 0.9$.

6. Conclusion

This study presents a robust finite element framework for modeling oncolytic virotherapy dynamics, successfully addressing the challenges of coupled nonlinear reaction-diffusion systems. Our analysis identifies viral replication rate (μ) and infection efficiency (β_3) as key therapeutic parameters, while revealing balanced competing effects in immune response factors (β_4, η_4). The developed method demonstrates consistent convergence and handles complex spatial patterns, with theoretical guarantees of solution existence and uniqueness in Sobolev spaces. The sensitivity analysis

provides clinically actionable insights for parameter prioritization in treatment optimization. This computational approach enables extension to multidimensional tumor geometries and combination therapies, offering a foundation for personalized treatment planning. We also intend to focus on adaptive discontinuous Galerkin methods, investigating hp-refinement strategies, efficient error estimators, and dynamic mesh adaptation to enhance accuracy and computational efficiency for problems with discontinuities or complex features. Relevant advanced numerical techniques for adaptive discontinuous Galerkin methods can be found in [9, 10, 16].

References

[1] O. T. Al-Bairaqdar, Y. A. Sabawi, and M. S. Hasso, *Efficient numerical solution of the Allen–Cahn equation via a non-lumping Galerkin finite element method*, AIP Advances, *15*(7) (2025).

[2] N. Atouani and K. Omrani, *Galerkin finite element method for the Rosenau-RLW equation*, Computers & Mathematics with Applications, *66*(3) (2013), 289–303.

[3] S. Kyun Chung and S. Nam Ha, *Finite element Galerkin solutions for the Rosenau equation*, Applicable Analysis, *54*(1-2) (1994), 39–56.

[4] A. M. Elaiw, A. D. Hobiny, and A. D. Al Agha, *Global dynamics of reaction-diffusion oncolytic M1 virotherapy with immune response*, Applied Mathematics and Computation, *367* (2020), 1–21.

[5] L. C. Evans, *Partial differential equations*, American Mathematical Society, Vol. 19, 2022.

[6] S. Kesavan, *Topics in functional analysis and applications*, (1989).

[7] E. Kreyszig, *Introductory functional analysis with applications*, John Wiley & Sons, Vol. 17, 1991.

[8] J. Malinzi, R. Ouifki, A. Eladdadi, D. F. M. Torres, and K. A. J. White, *Enhancement of chemotherapy using oncolytic virotherapy: mathematical and optimal control analysis*, Mathematical Biosciences and Engineering, *12*(6) (2015), 1435–1463.

[9] N. A. Mohammad, Y. A. Sabawi, and M. S. Hasso, *Numerical solution based on the Haar wavelet collocation method for partial integro-differential equations of Volterra type*, Arab Journal of Basic and Applied Sciences, *31*(1) (2024), 614–628.

[10] Najem A. Mohammad, Younis A. Sabawi, and Mohammad Sh. Hasso, *A compact finite-difference and Haar wavelets collocation technique for parabolic Volterra integro-differential equations*, Physica Scripta, *99*(12) (2024), 125251.

[11] A. Quarteroni and S. Quarteroni, *Numerical models for differential problems*, Vol. 2, Springer, 2009.

[12] H. M. Rasool, B. Faris Azeez, and M. A. Pirdawood, *A multifaceted study of COVID-19: stability analysis, numerical solution, and sensitivity analysis*, Eurasian Journal of Science and Engineering, *11*(3) (2025), 49–65.

[13] E. Ratajczyk, U. Ledzewicz, and H. Schättler, *Optimal control for a mathematical model of glioma treatment with oncolytic therapy and TNF-β inhibitors*, Journal of Optimization Theory and Applications, *176*(2) (2018), 456–477.

[14] X. Ren, Y. Tian, L. Liu, and X. Liu, *A reaction-diffusion within-host HIV model with cell-to-cell transmission*, Journal of Mathematical Biology, *76* (2018), 1831–1872.

[15] Y. Sabawi, M. I. Sadeeq, and M. Ameen, *Numerical solution of Burgers' equation using the explicit and Crank-Nicolson finite difference methods*, Eurasian Journal of Science and Engineering, *11*(3) (2025), 199–214.

[16] Y. A. Sabawi and H. Q. Hamad, *Numerical solution of the Whitham-Broer-Kaup shallow water equation by quartic B-spline collocation method*, Physica Scripta, *99*(1) (2024), 015242.

[17] Y. A. Sabawi and B. O. Hussen, *A cubic B-spline finite element method for Volterra integro-differential equation*, Palestine Journal of Mathematics, *13*(3) (2024), 571–583.

[18] M. I. Sadeeq and Y. A. Sabawi, *Cubic B-spline finite element method for solving Whitham-Broer-Kaup shallow water model*, International Journal of Computational Methods (2025).

[19] Y. Tao and Q. Guo, *The competitive dynamics between tumor cells, a replication competent virus and an immune response*, Journal of Mathematical Biology, *51*(1) (2005), 37–74.

[20] Vidar Thomée, *Galerkin Finite Element Methods for Parabolic Problems*, Springer Series in Computational Mathematics, 2nd ed., Springer-Verlag, Berlin, 2006.

[21] J. Tumwiine, J. Mugisha, and L. Luboobi, *On the global stability of the intra-host dynamics of malaria and the immune system*, Journal of Mathematical Analysis and Applications, *341* (2008), 855–869.
[22] Y. Wang, J. Tian, and J. Wei, *Lytic cycle: a defining process in oncolytic virotherapy*, Applied Mathematical Modelling, *37*(8) (2013), 5962–5978.
[23] Z. Wang, Z. Guo, and H. Peng, *Dynamical behavior of a new oncolytic virotherapy model based on gene variation*, Discrete and Continuous Dynamical Systems - Series S, *10*(5) (2017), 1079–1093.